

Effect of Redshift Distributions of Fast Radio Bursts on Cosmological Constraints

Da-Chun Qiang* and Hao Wei†

School of Physics, Beijing Institute of Technology, Beijing 100081, China

ABSTRACT

Nowadays, fast radio bursts (FRBs) have been a promising probe for astronomy and cosmology. However, it is not easy to identify the redshifts of FRBs to date. Thus, no sufficient actual FRBs with identified redshifts can be used to study cosmology currently. In the past years, one has to use the simulated FRBs with “known” redshifts instead. To simulate an FRB, one should randomly assign a redshift to it from a given redshift distribution. But the actual redshift distribution of FRBs is still unknown so far. Therefore, many redshift distributions have been assumed in the literature. In the present work, we study the effect of various redshift distributions on cosmological constraints, while they are treated equally. We find that different redshift distributions lead to different cosmological constraining abilities from the simulated FRBs. This result emphasizes the importance to find the actual redshift distribution of FRBs, and reminds us of the possible bias in the FRB simulations due to the redshift distributions.

PACS numbers: 98.80.Es, 98.70.Dk, 98.80.-k

* email address: 875019424@qq.com

† Corresponding author; email address: haowei@bit.edu.cn

I. INTRODUCTION

Currently, fast radio bursts (FRBs) have become a thriving field in astronomy and cosmology [1–12]. Since their first discovery [13, 14], an extragalactic/cosmological origin is strongly suggested to FRBs, due to the large dispersion measure (DM) of observed FRBs well in excess of the Galactic value. To date, the redshifts of several FRBs have been identified by the precise localizations of their host galaxies [15–22]. For example, the redshift of the first known repeating FRB (namely FRB 121102) has been identified as $z = 0.19273$ [15]. Currently, FRB 190523 has the largest identified redshift $z = 0.66$ [17]. The 12 FRBs with identified redshifts as of November 2020 were summarized in e.g. [23]. Clearly, they are all at cosmological distances. Therefore, it is justified and well motivated to study cosmology by using FRBs. We refer to e.g. [24–40] for some interesting works on the FRB cosmology.

As is well known, one of the key observational quantities of FRBs is the dispersion measure DM. The radio signals of different frequencies from FRB reach earth at different times, due to the cold plasma along the path. According to e.g. [41], in the rest frame, an electromagnetic signal propagates through an ionized medium (plasma) with a velocity less than the speed of light in vacuum c , and hence this signal of frequency $\nu \gg \nu_p$ is delayed relative to a signal in vacuum by a time proportional to ν^{-2} and the column density of the free electrons, where ν_p is the plasma frequency. In practice, it is convenient to measure the time delay Δt in the observer frame between two signals of frequencies ν_1 and ν_2 . Taking the redshift effect into account, this time delay is given by [24, 25, 35, 36, 42, 43]

$$\Delta t = \frac{e^2}{2\pi m_e c} \left(\frac{1}{\nu_1^2} - \frac{1}{\nu_2^2} \right) \int \frac{n_{e,z}}{1+z} dl \equiv \frac{e^2}{2\pi m_e c} \left(\frac{1}{\nu_1^2} - \frac{1}{\nu_2^2} \right) \text{DM}, \quad (1)$$

where $n_{e,z}$ is the number density of free electrons in the medium (given in units of cm^{-3}) at redshift z , m_e and e are the mass and charge of electron, respectively. Using Eq. (1), one can get the column density of the free electrons $\text{DM} \equiv \int n_{e,z}/(1+z) dl$ by measuring the time delay Δt between two signals of frequencies ν_1 and ν_2 . It is worth noting that the distance dl along the path in DM records the expansion history of the universe. Therefore, DM plays a key role in the FRB cosmology.

Clearly, the observed DM of FRB can be separated into [24–28, 35–38]

$$\text{DM}_{\text{obs}} = \text{DM}_{\text{MW}} + \text{DM}_{\text{IGM}} + \text{DM}_{\text{HG}}, \quad (2)$$

where DM_{MW} , DM_{IGM} , and DM_{HG} are the contributions from the Milky Way, the intergalactic medium (IGM), and the host galaxy (HG, including interstellar medium of HG and the near-source plasma), respectively. Since thousands of pulsars in the Milky Way and the Small/Large Magellanic Clouds were observed, one can reliably infer the density distribution of the free electrons in or nearby the Milky Way from the observed DMs of these pulsars. So, for a well-localized FRB, the corresponding DM_{MW} can be estimated with reasonable certainty by using the well-known tools NE2001 [44, 45] or YMW16 [46]. Thus, subtracting the “known” DM_{MW} from DM_{obs} in Eq. (2), it is convenient to introduce the extragalactic DM of an FRB as the observed quantity [25, 28, 35–37],

$$\text{DM}_{\text{E}} \equiv \text{DM}_{\text{IGM}} + \text{DM}_{\text{HG}}. \quad (3)$$

The main contribution to DM of FRB comes from IGM. In fact, DM_{IGM} carries the key information about IGM and the cosmic expansion history. In principle, one can constrain cosmological models by using the observed DM_{E} of a large number of FRBs with identified redshifts.

Unfortunately, it is not so easy to identify the redshifts of FRBs to date. Since the first discovery of FRB [13, 14], the redshifts have been identified only for 12 extragalactic FRBs, as is summarized in e.g. [23]. Therefore, no sufficient actual FRBs with identified redshifts can be used to study cosmology currently. In the past years, one has to use the simulated FRBs with “known” redshifts instead. The devil is in the details. To simulate an FRB, one should randomly assign a redshift to it from a given redshift distribution. However, the actual redshift distribution of FRBs is still unknown to date. Therefore, various redshift distributions have been assumed in the literature, while some of them are motivated by the star formation history/rate [61, 65, 88, 89] or compact binary mergers [88] and so on, some of them are borrowed from other objects such as gamma-ray bursts (GRBs) [25–27, 34, 35, 38], some of them come from the observed FRBs (such as Burr and Burr12 proposed in this work), and some of them are

not well motivated at all (e.g. Uniform). In the present work, we are interested to see whether or not various redshift distributions used to simulate FRBs can affect cosmological constraints considerably, and we do not care whether these redshift distributions are well motivated or where they come from. Our goal is just to see how they affect the cosmological constraints, while they are treated equally in this work, no matter whether they are the intrinsic ones or the observed ones.

The rest of this paper is organized as follows. In Sec. II, we introduce various redshift distributions for FRBs considered extensively in the literature. In addition, we also propose two new redshift distributions inferred from the actual FRBs data to date, which are fairly different from the existing ones in the literature. In Sec. III, we briefly describe the key points to simulate FRBs. In Sec. IV, we constrain various cosmological models by using these simulated FRBs, and try to see the effect of redshift distributions on cosmological constraints. In Sec. V, some brief concluding remarks are given.

II. VARIOUS REDSHIFT DISTRIBUTIONS FOR FRBS

A. New redshift distributions

In the literature, various redshift distributions for FRBs have been extensively considered. To our best knowledge, (almost) all of them are not inferred from the actual FRBs data. So, let us try it at first. Note that an online catalogue of the observed FRBs can be found in FRBCAT [47], which summarizes almost all observational aspects concerning the published FRBs. As of January 2021, FRBCAT catalogue contains 129 observed FRBs. Of course, most of them have no identified redshifts. However, one can roughly infer the redshift from the observed DM of FRB, following the methodology described in e.g. Sec. 2.2 of [48]. Since this is an inferred redshift, we do not require a high precision, and hence we can slightly simplify the methodology of [48]. For an observed FRB, its DM_{obs} can be separated into three components as in Eq. (2). One can directly read its DM_{MW} from FRBCAT [47], which is estimated by using NE2001 [44, 45] or YMW16 [46]. On the other hand, one can assume $DM_{\text{HG}} = 50/(1+z)$ pc cm⁻³ following e.g. [48, 49]. The mean DM_{IGM} can be estimated by $DM_{\text{IGM}} = 3cH_0\Omega_b/(8\pi Gm_p) \int_0^z (f_{\text{IGM}}(\tilde{z})f_e(\tilde{z})(1+\tilde{z})/E(\tilde{z})) d\tilde{z}$ (see e.g. [24, 25, 35–38, 48]), in which one can assume the simplest flat Λ CDM cosmology to estimate $E(z) = (\Omega_m(1+z)^3 + (1-\Omega_m))^{1/2}$ and adopt the values of Ω_m , Ω_b , H_0 from Planck 2018 results [50], while $f_{\text{IGM}} = 0.83$ and $f_e = 7/8$ as in e.g. [24–26, 28, 35]. So, the right hand side of Eq. (2) becomes an explicit function of redshift z . For an observed FRB, one can infer its redshift z by numerically solving Eq. (2) with the observational value of DM_{obs} . Of course, we stress that it is just a roughly inferred redshift only for reference. Following this methodology, now we have 129 actual FRBs with inferred redshifts. To get a reasonable redshift distribution, we need an anchor. Very recently, FRB 200428 in our Milky Way was observed (see e.g. [51–54]). So, we also take this FRB at $z = 0$ into account. We fit these 130 actual FRBs with the **fitter** Python package [55], which can find the most probable distribution(s) for a given data sample by using 80 distributions in SciPy [56]. Finally, we obtain the best redshift distribution for these 130 actual FRBs, namely Burr distribution [57] (note that Burr Type III distribution is called Burr distribution for short in SciPy). The standardized Burr distribution is given by [57]

$$f_{\text{Burr}}(x, b, k) = \frac{bk x^{-b-1}}{(1+x^{-b})^{k+1}}, \quad (4)$$

where $x \geq 0$, $b > 0$ and $k > 0$. One can shift and/or scale this distribution by using the shift and scale parameters (ℓ and s), namely [57]

$$P_{\text{Burr}}(z, b, k, \ell, s) = f_{\text{Burr}}((z - \ell)/s, b, k) / s. \quad (5)$$

The best parameters for the 130 actual FRBs mentioned above are $b = 2.8733$, $k = 0.4568$, $\ell = -0.0043$ and $s = 0.7357$. We present this best Burr distribution in the left panel of Fig. 1.

As mentioned above, there are 12 extragalactic FRBs with identified redshifts to date, as is summarized in e.g. Table 2 of [23]. Eleven of them are also compiled in the above 129 FRBs catalogue, while FRB 200430 is not. We replace the inferred redshifts of these 11 FRBs by the actually identified ones, and also take FRB 200430 into account. Similarly, we fit these 131 FRBs with the **fitter** Python package [55],

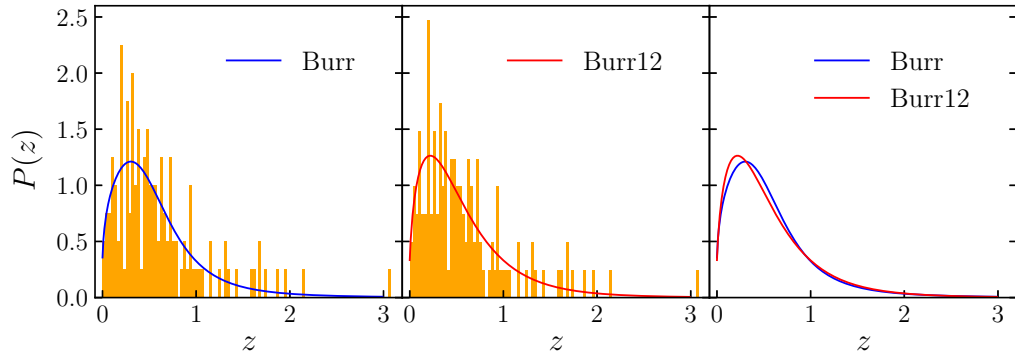


FIG. 1: Left panel: The best Burr distribution (blue solid line) as a function of redshift z versus the normalized histogram of 129 actual FRBs with inferred redshifts plus a Galactic FRB 200428 at $z = 0$. Middle panel: The best Burr Type XII distribution (red solid line) as a function of redshift z versus the normalized histogram of 118 actual FRBs with inferred redshifts and 12 actual FRBs with observed redshifts plus a Galactic FRB 200428 at $z = 0$. Right panel: Comparison of the best Burr and Burr Type XII distributions. See Sec. II A for details.

and then obtain the best redshift distribution, namely Burr Type XII distribution (Burr12) [58]. The standardized Burr Type XII distribution is given by [58]

$$f_{\text{Burr12}}(x, b, k) = \frac{bk x^{b-1}}{(1+x^b)^{k+1}}, \quad (6)$$

where $x \geq 0$, $b > 0$ and $k > 0$. One can shift and/or scale this distribution by using the shift and scale parameters (ℓ and s), namely [58]

$$P_{\text{Burr12}}(z, b, k, \ell, s) = f_{\text{Burr12}}((z - \ell)/s, b, k) / s. \quad (7)$$

The best parameters for the 131 actual FRBs mentioned above are $b = 1.4653$, $k = 3.9060$, $\ell = -0.0064$ and $s = 1.3963$. We present this best Burr Type XII distribution in the middle panel of Fig. 1.

We compare the best Burr and Burr12 distributions obtained above in the right panel of Fig. 1. It is easy to see that they are fairly close in fact. We stress that these two new redshift distributions Burr and Burr12 are not the actual one of FRBs, since the inferred redshifts are rough, while the 129 observed FRBs from FRBCAT are collected from many different telescopes with different sensitivities, band widths, central frequencies, fields of view, and operation times. Thus, many selection effects exist in these 129 observed FRBs (we thank the referee for pointing out this issue). On the other hand, these two new redshift distributions Burr and Burr12 are the observed ones, which are different from the intrinsic ones. One should be aware of this. However, as mentioned in Sec. I, our goal is just to see how redshift distributions affect the cosmological constraints, and hence they are treated equally in this work, no matter whether they are the intrinsic ones or the observed ones, and we do not care whether these redshift distributions are well motivated or where they come from. So, Burr and Burr12 do not have any special position. Let us be very clear that they are just trivial two in all the 9 redshift distributions considered equally in this work.

B. Existing redshift distributions

In fact, many existing redshift distributions for FRBs have been extensively considered in the literature. Note that they do not come from the actual FRBs. Since the actual redshift distribution of FRBs is still unknown to date, one might borrow the ones of other objects. For example, in e.g. [25–27, 34, 35, 38], one can argue that FRBs are similar/related to gamma-ray bursts (GRBs), and hence assume that the redshift distribution of FRBs takes the one of GRBs [59] (termed “PzGRB”), namely

$$P_{\text{GRB}}(z) \propto z e^{-z}, \quad (8)$$

which is a special case of Erlang distribution [60]. PzGRB was used extensively in the literature.

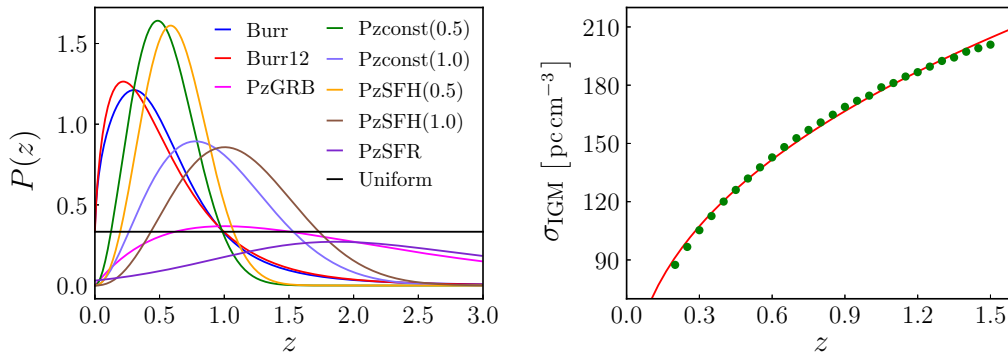


FIG. 2: Left panel: The 9 normalized redshift distributions for FRBs. See Sec. II for details. Right panel: σ_{IGM} versus redshift z . The 27 green dots are reproduced from the bottom panel of Fig. 1 of [72]. The red solid line is plotted according to Eq. (16). See Sec. III for details.

In e.g. [61], two redshift distributions for FRBs were proposed. The first one (termed “Pzconst”) assumes that FRBs have a constant comoving number density, and the corresponding redshift distribution function is given by [61]

$$P_{\text{const}}(z) \propto \frac{d_C^2(z)}{(1+z)H(z)} \exp\left(-\frac{d_L^2(z)}{2d_L^2(z_{\text{cut}})}\right), \quad (9)$$

where $H(z)$ is the Hubble parameter, $d_C(z) = d_L(z)/(1+z) = c \int_0^z d\tilde{z}/H(\tilde{z})$ is the comoving distance, $d_L(z)$ is the luminosity distance. Gaussian cutoff at z_{cut} is introduced to represent an instrumental signal-to-noise threshold. The second one (termed “PzSFH”) assumes that FRBs follow the star-formation history (SFH) [62], whose density is given by

$$\dot{\rho}_*(z) = \frac{(b_1 + b_2 z) h}{1 + (z/b_3)^{b_4}}, \quad (10)$$

with $b_1 = 0.0170$, $b_2 = 0.13$, $b_3 = 3.3$, $b_4 = 5.3$ and $h = 0.7$ [61, 63, 64]. In this case, the SFH-based redshift distribution function reads [61]

$$P_{\text{SFH}}(z) \propto \frac{\dot{\rho}_*(z) d_C^2(z)}{(1+z)H(z)} \exp\left(-\frac{d_L^2(z)}{2d_L^2(z_{\text{cut}})}\right). \quad (11)$$

In the literature, the cutoff z_{cut} has been set to various values. In [61] and e.g. [36, 40], $z_{\text{cut}} = 0.5$ was adopted. On the other hand, $z_{\text{cut}} = 1.0$ was considered in e.g. [31, 37]. We call the corresponding redshift distributions “Pzconst(0.5)”, “Pzconst(1.0)”, “PzSFH(0.5)”, “PzSFH(1.0)”, respectively.

Another type of redshift distribution for FRBs was proposed in e.g. [65]. One might argue that the distribution of FRBs closely trace the cosmic star-formation rate (SFR) for young stellar FRB progenitors. In e.g. [66], the cosmic SFR function is given by

$$\psi(z) = \frac{0.015(1+z)^{2.7}}{1 + ((1+z)/2.9)^{5.6}} M_{\odot} \text{ yr}^{-1} \text{ Mpc}^{-3}. \quad (12)$$

The appropriately weighted redshift distribution is obtained by considering the quantity [65]

$$\zeta_{\text{SFR}} = \frac{\int_0^z \psi(\tilde{z}) d\tilde{z}}{\int_0^{z_{\text{max}}} \psi(\tilde{z}) d\tilde{z}}, \quad (13)$$

and drawing it as a uniform random number between 0 and 1. Since the right hand side of Eq. (13) is an explicit function of redshift z , for any uniform random number $0 \leq \zeta_{\text{SFR}} \leq 1$, one can obtain the corresponding redshift z by numerically solving Eq. (13). So, the SFR-based redshift distribution

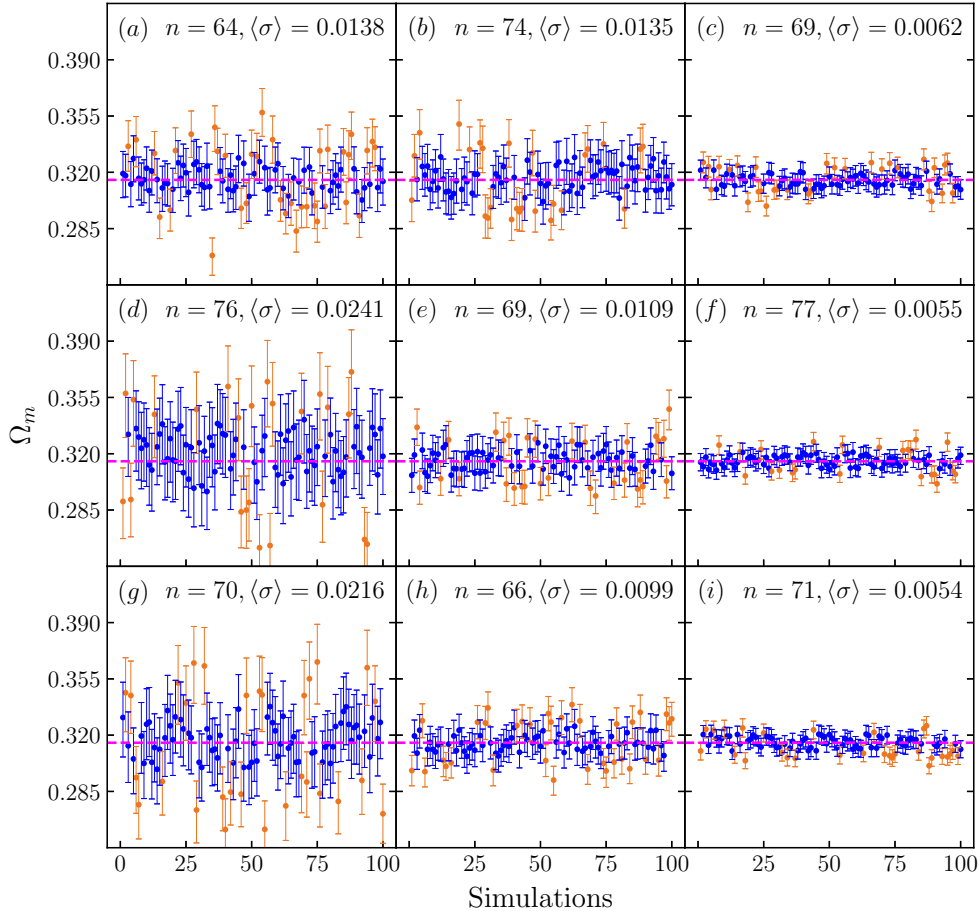


FIG. 3: Panels (a) to (i) correspond to the redshift distributions Burr, Burr12, PzGRB, Pzconst(0.5), Pzconst(1.0), PzSFR, PzSFH(0.5), PzSFH(1.0), and Uniform, respectively. In each panel, the marginalized 1σ constraints on the cosmological parameter Ω_m of the flat Λ CDM model for 100 simulations are presented. In each simulation, $N_{\text{FRB}} = 1000$ FRBs are generated by using the flat Λ CDM model with the preset parameter $\Omega_m = 0.3153$ (indicated by the magenta dashed lines). The blue means with error bars (the chocolate means with error bars) indicate that the preset $\Omega_m = 0.3153$ is consistent (inconsistent) with the simulated FRBs within 1σ region, respectively. n and $100 - n$ are the numbers of blue and chocolate means with error bars, respectively. $\langle\sigma\rangle$ is the mean of the uncertainties of 100 constraints on the cosmological parameter Ω_m . See Sec. IV for details.

(termed “PzSFR”) can be generated for FRBs. In principle, z_{max} can be set to any value, and then PzSFR generates random redshifts in the range of $0 \leq z \leq z_{\text{max}}$.

Naively, since there is no guideline for the redshift distribution of FRBs to date, it is also reasonable to just consider a uniform distribution. One can uniformly assign a random redshift z from 0 to z_{max} . In the present work, we also take this uniform redshift distribution into account.

In the left panel of Fig. 2, we summarize the 9 redshift distributions for FRBs, which are all normalized. Notice that the distributions Pzconst and PzSFH are plotted just for demonstration by assuming the simplest flat Λ CDM cosmology with $\Omega_m = 0.3153$ taken from Planck 2018 results [50]. We stress that there are other types of redshift distributions for FRBs in the literature. We do not try to consider all redshift distributions for FRBs in a limited work. With these 9 redshift distributions, we simulate FRBs and then try to see the effect of redshift distributions for FRBs on cosmological constraints.

III. SIMULATING FRBS

Here, we briefly describe the key points to simulate FRBs. As mentioned in Sec. I, we consider the extragalactic DM defined in Eq. (3) as the observed quantity. The main contribution comes from IGM.

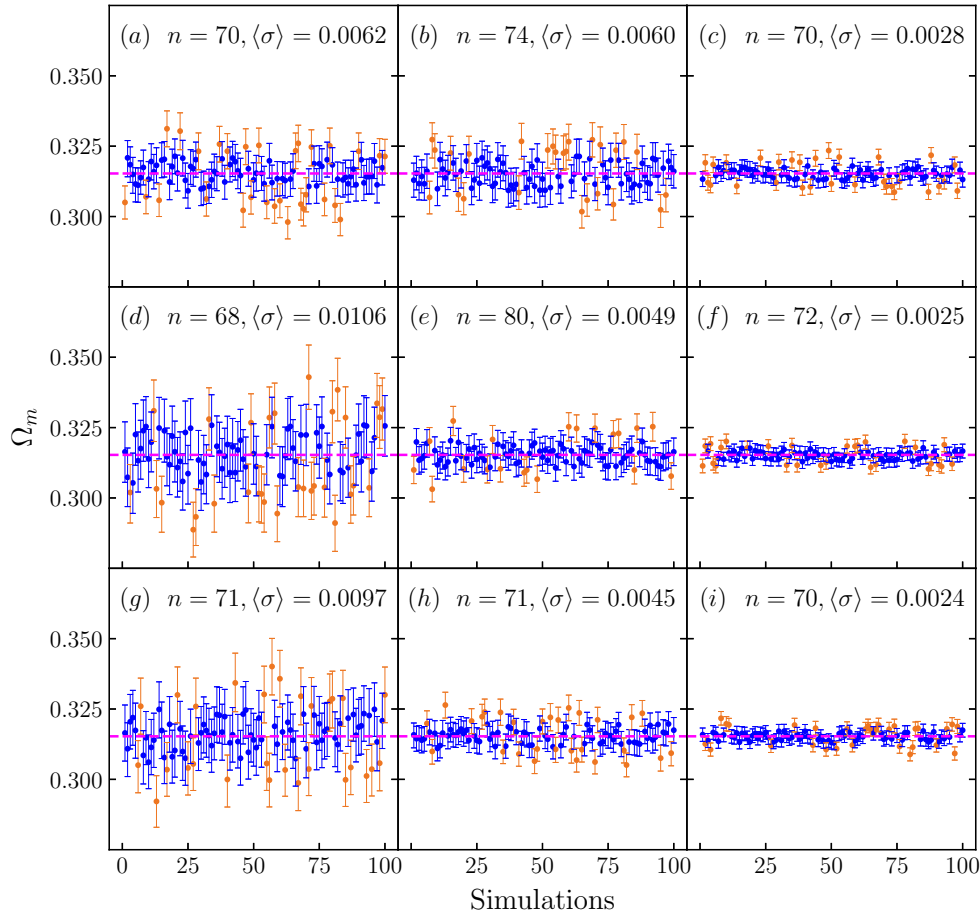


FIG. 4: The same as in Fig. 3, but $N_{\text{FRB}} = 5000$ in each simulation.

As is shown in e.g. [24, 25, 35–38], the mean of DM_{IGM} is given by

$$\langle \text{DM}_{\text{IGM}} \rangle = \frac{3cH_0\Omega_b}{8\pi Gm_p} \int_0^z \frac{f_{\text{IGM}}(\tilde{z}) f_e(\tilde{z}) (1 + \tilde{z}) d\tilde{z}}{E(\tilde{z})}, \quad (14)$$

where Ω_b is the present fractional density of baryons, m_p is the mass of proton, H_0 is the Hubble constant, $E \equiv H/H_0$ is the dimensionless Hubble parameter. f_{IGM} is the fraction of baryon mass in IGM, which is a function of redshift z in principle [36–38]. Following e.g. [25, 26, 28, 35], here we adopt a constant $f_{\text{IGM}} = 0.83$ (see e.g. [67, 68] and [24]). The ionized electron number fraction per baryon is

$$f_e(z) \equiv Y_{\text{H}} \chi_{e,\text{H}}(z) + \frac{1}{2} Y_{\text{He}} \chi_{e,\text{He}}(z), \quad (15)$$

in which hydrogen (H) and helium (He) mass fractions are $Y_{\text{H}} = (3/4)y_1$ and $Y_{\text{He}} = (1/4)y_2$, where $y_1 \sim 1$ and $y_2 \simeq 4 - 3y_1 \sim 1$ are the hydrogen and helium mass fractions normalized to the typical values 3/4 and 1/4, respectively. In principle, the ionization fractions $\chi_{e,\text{H}}(z)$ and $\chi_{e,\text{He}}(z)$ are both functions of redshift z . It is expected that intergalactic hydrogen and helium are fully ionized at redshifts $z \lesssim 6$ and $z \lesssim 3$ [69, 70] (see also e.g. [71, 86]), respectively. Thus, for FRBs at redshifts $z \leq 3$, they are both fully ionized, namely $\chi_{e,\text{H}}(z) = \chi_{e,\text{He}}(z) = 1$. So, $f_e(z) \simeq 7/8$ for $z \leq 3$.

Note that DM_{IGM} will deviate from the mean $\langle \text{DM}_{\text{IGM}} \rangle$ if the plasma density fluctuations are taken into account [72] (see also e.g. [32, 42]). The uncertainty σ_{IGM} was studied in e.g. [72], where three models for halo gas profile of the ionized baryons were used. Following e.g. [36], we consider the simplest one, namely the top hat model, and the corresponding σ_{IGM} was given by the green dots in the bottom panel of Fig. 1 of [72]. It is easy to fit these 27 green dots with a simple power-law function [36]

$$\sigma_{\text{IGM}}(z) = 173.8 z^{0.4} \text{ pc cm}^{-3}. \quad (16)$$

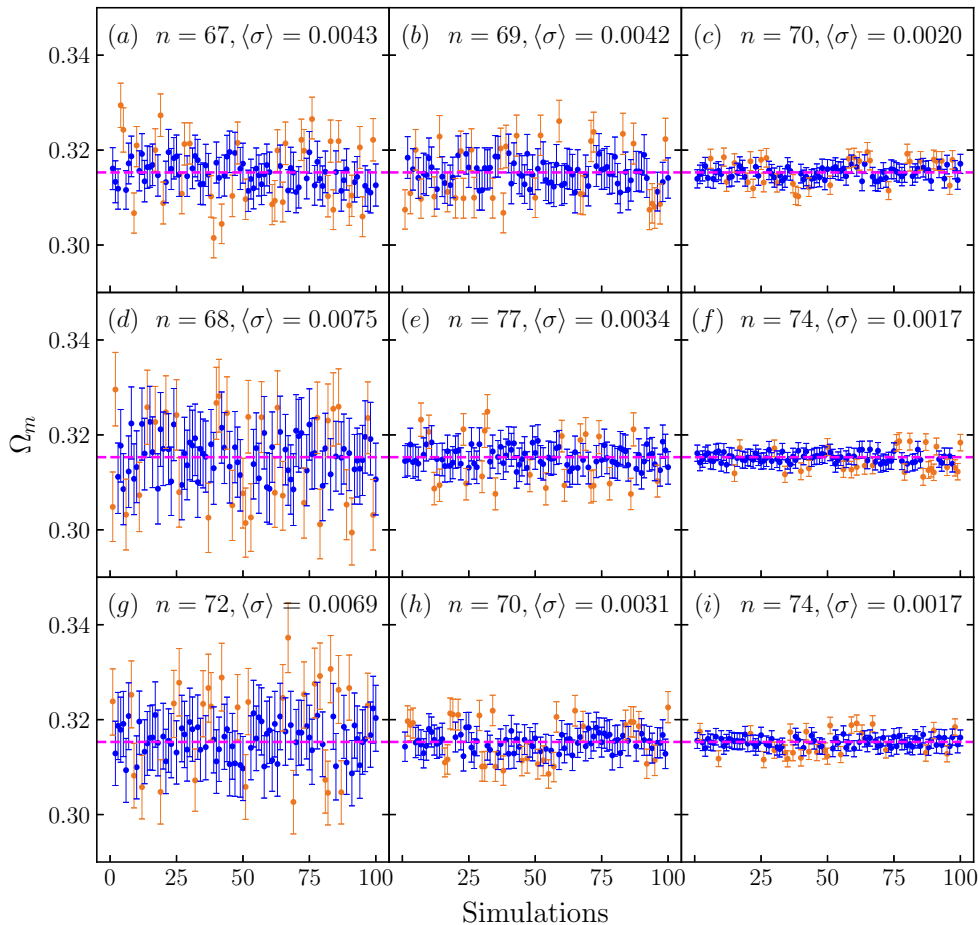


FIG. 5: The same as in Fig. 3, but $N_{\text{FRB}} = 10000$ in each simulation.

In the right panel of Fig. 2, we reproduce these 27 green dots from [72], and also plot the power-law $\sigma_{\text{IGM}}(z)$ given by Eq. (16). Obviously, they coincide with each other fairly well.

The contribution from the host galaxy of FRB, i.e. DM_{HG} , is poorly known. The observed DM_{HG} for an FRB at redshift z is given by (e.g. [25–28, 35–37])

$$\text{DM}_{\text{HG}} = \text{DM}_{\text{HG,loc}}/(1+z), \quad (17)$$

where $\text{DM}_{\text{HG,loc}}$ is the local DM of FRB host galaxy. Following e.g. [28, 35, 36], we reasonably assume that $\text{DM}_{\text{HG,loc}}$ is independent of redshift z .

We briefly describe the steps to generate the simulated FRBs with “known” redshifts. At first, we assign a random redshift z_i to the i -th simulated FRB from a given redshift distribution (one of the nine mentioned in Sec. II). In this step, the distributions Pzconst and PzSFH should use a given cosmology characterized by $E(z) = H(z)/H_0$ (which will be specified in Sec. IV) to calculate the comoving and luminosity distances, while the other distributions should not. As mentioned above, both the intergalactic hydrogen and helium are fully ionized at $z \leq 3$, and hence we choose to generate the FRB redshifts in the range of $0 \leq z_i \leq 3$ (namely $z_{\text{max}} = 3$). The second step is to randomly assign $\text{DM}_{\text{IGM},i}$ and its uncertainty $\sigma_{\text{IGM},i} = \sigma_{\text{IGM}}(z_i)$ to this simulated FRB from a Gaussian distribution,

$$\text{DM}_{\text{IGM},i} = \mathcal{N}(\langle \text{DM}_{\text{IGM}} \rangle(z_i), \sigma_{\text{IGM}}(z_i)). \quad (18)$$

Here, $\langle \text{DM}_{\text{IGM}} \rangle(z_i)$ in Eq. (14) is calculated by using a given cosmology characterized by $E(z)$ (which will be specified in Sec. IV), and $\sigma_{\text{IGM}}(z_i)$ is calculated by using Eq. (16). The third step is to assign $\text{DM}_{\text{HG},i} = \text{DM}_{\text{HG,loc},i}/(1+z_i)$ and its uncertainty $\sigma_{\text{HG},i} = \sigma_{\text{HG,loc},i}/(1+z_i)$ to this simulated FRB,

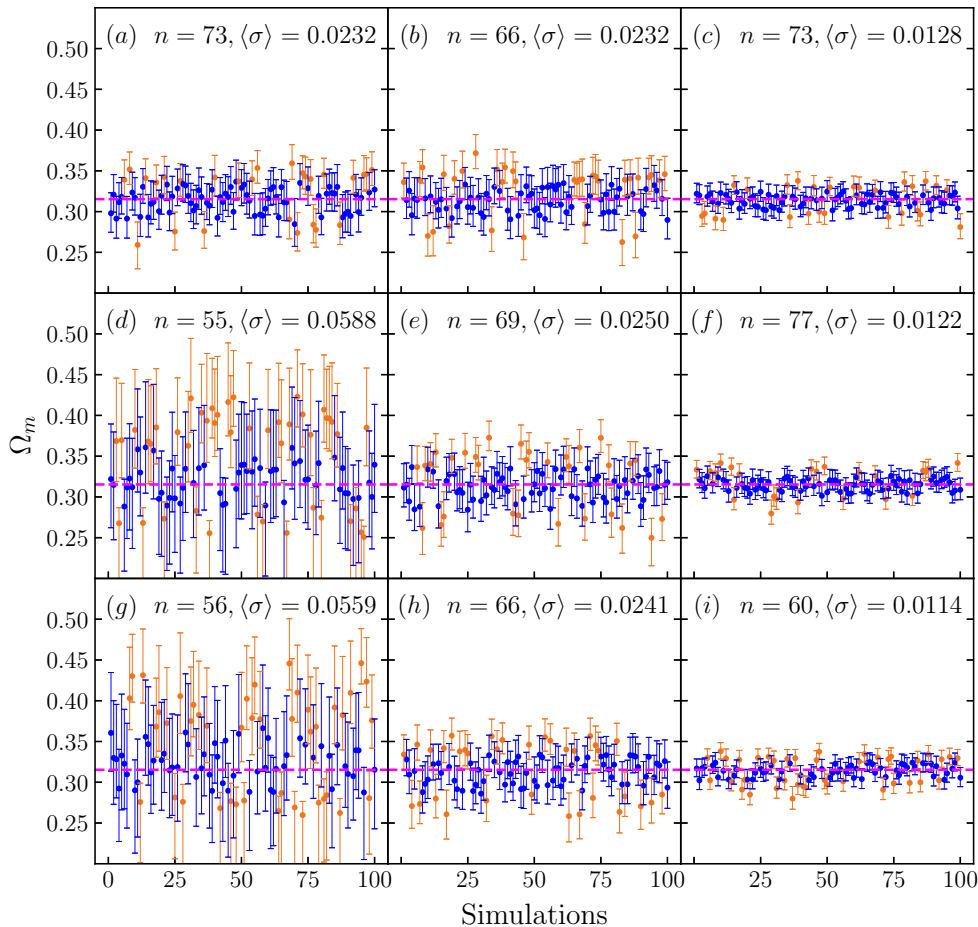


FIG. 6: The same as in Fig. 3, but in each simulation $N_{\text{FRB}} = 5000$ FRBs are generated by using the flat w CDM model with the preset cosmological parameters $\Omega_m = 0.3153$ and $w = -0.95$. The marginalized 1σ constraints are on the cosmological parameter Ω_m .

according to Eq. (17) and following e.g. [25–28, 35–37]. Here, $\text{DM}_{\text{HG}, \text{loc}, i}$ can be randomly assigned from a Gaussian distribution with the mean $\langle\text{DM}_{\text{HG}, \text{loc}}\rangle$ and a fluctuation $\sigma_{\text{HG}, \text{loc}}$ [25–28, 35–37], namely

$$\text{DM}_{\text{HG}, \text{loc}, i} = \mathcal{N}(\langle\text{DM}_{\text{HG}, \text{loc}}\rangle, \sigma_{\text{HG}, \text{loc}}), \quad (19)$$

while $\sigma_{\text{HG}, \text{loc}, i} = \sigma_{\text{HG}, \text{loc}}$. In the literature, $\text{DM}_{\text{HG}, \text{loc}} = 50 \text{ pc cm}^{-3}$ is frequently used (see e.g. [22, 48, 49]). On the other hand, it was argued in [73] that the median of $\text{DM}_{\text{HG}, \text{loc}}$ is about $30 \sim 70 \text{ pc cm}^{-3}$, while the uncertainty 20 pc cm^{-3} was frequently used in the literature (e.g. [25, 35, 36]). So, we adopt the fiducial values $\langle\text{DM}_{\text{HG}, \text{loc}}\rangle = 50 \text{ pc cm}^{-3}$ and $\sigma_{\text{HG}, \text{loc}} = 20 \text{ pc cm}^{-3}$ in this work. Finally, the simulated DM_{E} data and its uncertainty for the i -th simulated FRB are given by

$$\text{DM}_{\text{E}, i} = \text{DM}_{\text{IGM}, i} + \text{DM}_{\text{HG}, i}, \quad \text{and} \quad \sigma_{\text{E}, i} = (\sigma_{\text{IGM}, i}^2 + \sigma_{\text{HG}, i}^2)^{1/2}. \quad (20)$$

One can repeat the above steps for N_{FRB} times to generate N_{FRB} simulated FRBs.

The lower-limit estimates for the number of FRB events are a few thousands per sky per day [3, 74]. Even conservatively, the all-sky burst rate floor derived from the pre-commissioning of CHIME/FRB is 3×10^2 events per day [75]. Several projects designed to detect and localize FRBs with arcsecond accuracy in real time are under construction or in commission, for example DSA-10 [76], DSA-2000 [77], MeerKAT [78], UTMOST-2D [79], and LOFAR [80]. It is reasonable to expect that numerous FRBs with identified redshifts will become available in the future. Therefore, N_{FRB} can be fairly large, for example $\mathcal{O}(10^3)$ or even more.

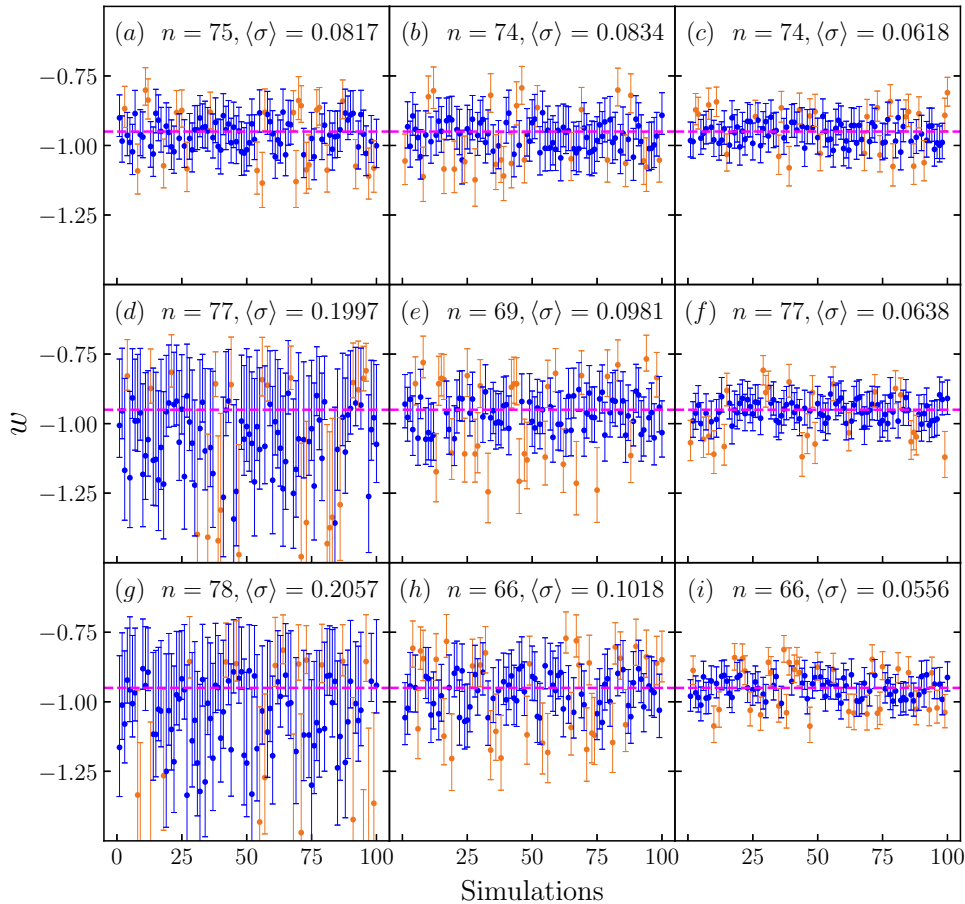


FIG. 7: The same as in Fig. 6, but the marginalized 1σ constraints are on the cosmological parameter w .

IV. COSMOLOGICAL CONSTRAINTS FROM THE SIMULATED FRBS

Now, we consider the constraints on various cosmological models from the simulated FRBs. For a specified cosmological model, its dimensionless Hubble parameter $E(z) = H(z)/H_0$ is given. So, one can calculate the theoretical extragalactic DM of an FRB by using

$$\text{DM}_E^{\text{th}}(z) = \langle \text{DM}_{\text{IGM}} \rangle(z) + \langle \text{DM}_{\text{HG, loc}} \rangle / (1+z), \quad (21)$$

where $\langle \text{DM}_{\text{IGM}} \rangle(z)$ is given by Eq. (14), and the universal constant $\langle \text{DM}_{\text{HG, loc}} \rangle$ is a model parameter for HG. The model parameters can be constrained by performing a χ^2 analysis, while

$$\chi^2 = \sum_i \frac{(\text{DM}_{E,i} - \text{DM}_E^{\text{th}}(z_i))^2}{\sigma_{E,i}^2}. \quad (22)$$

In this work, we use the Markov Chain Monte Carlo (MCMC) code **CosmoMC** [81] to this end. Since we are mainly interested in the effect of redshift distributions on cosmological constraints, to save the length of paper, we do not present the constraints on HG parameter $\langle \text{DM}_{\text{HG, loc}} \rangle$ in the following, although they are also available in fact.

At first, we consider the simplest cosmological model, namely the flat Λ CDM model. In this case, the dimensionless Hubble parameter is given by (e.g. [82, 83])

$$E(z) = (\Omega_m(1+z)^3 + (1-\Omega_m))^{1/2}, \quad (23)$$

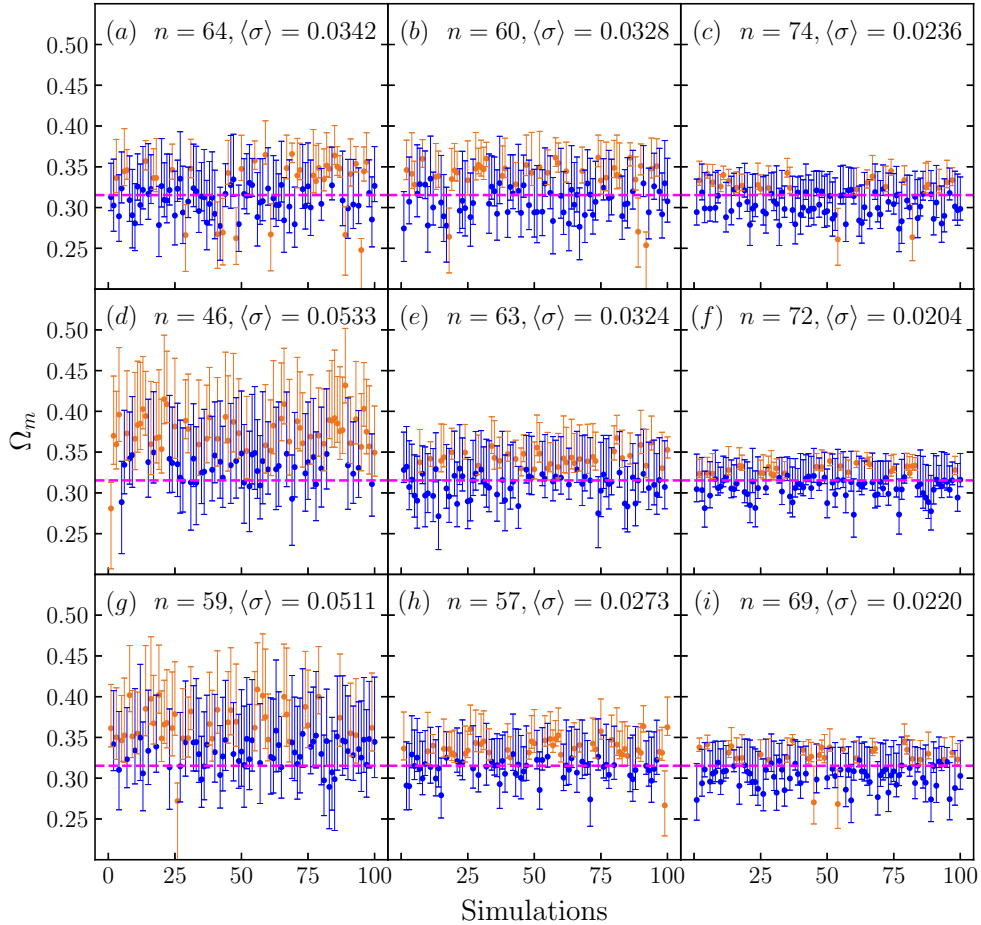


FIG. 8: The same as in Fig. 3, but in each simulation $N_{\text{FRB}} = 5000$ FRBs are generated by using the flat CPL model with the preset cosmological parameters $\Omega_m = 0.3153$, $w_0 = -0.95$ and $w_a = -0.3$. The marginalized 1σ constraints are on the cosmological parameter Ω_m .

where Ω_m is the only free cosmological parameter. We simulate N_{FRB} FRBs with the preset cosmological parameter $\Omega_m = 0.3153$ taken from Planck 2018 results [50]. Then, we constrain the flat Λ CDM model with these simulated FRBs. To avoid the statistical noise due to random fluctuations, one should repeat the constraints for a large number of simulations. However, it is fairly expensive to consider too many simulations since they consume a large amount of computation power and time. As a balance, we choose to consider 100 simulations, which is enough in fact.

In Fig. 3, the marginalized 1σ constraints on the cosmological parameter Ω_m of the flat Λ CDM model for 100 simulations are presented. In each simulation, $N_{\text{FRB}} = 1000$ FRBs are generated. It is easy to see from Fig. 3 that the preset parameter $\Omega_m = 0.3153$ can be found within 1σ region in most of the 100 simulations ($64 \sim 77\%$), for all cases of the 9 redshift distributions introduced in Sec. II. This implies that the cosmological constraints from simulated FRBs are fairly reliable and robust. However, the uncertainties of the constraints are different. Using the naked eye, we find from Fig. 3 that the error bars of right panels (c), (f), (i) are shortest, the ones of bottom-left panels (d), (g) are longest, and the ones of other four panels (a), (b), (e), (h) are moderate. Quantitatively, $\langle\sigma\rangle$ in each panel gives the mean of the uncertainties of 100 constraints. Using $\langle\sigma\rangle$ in Fig. 3, we confirm that the cosmological constraints from FRBs simulated with the redshift distributions (c) PzGRB, (f) PzSFR, (i) Uniform are tightest, the ones with the redshift distributions (d) Pzconst(0.5), (g) PzSFH(0.5) are loosest, and the ones with the redshift distributions (a) Burr, (b) Burr12, (e) Pzconst(1.0), (h) PzSFH(1.0) are moderate. Clearly, they are separated into three distinct groups.

In Figs. 4 and 5, the number of simulated FRBs increases to $N_{\text{FRB}} = 5000$ and 10000, respectively. Clearly, the cosmological constraints become tighter when the number of simulated FRBs increases, for all

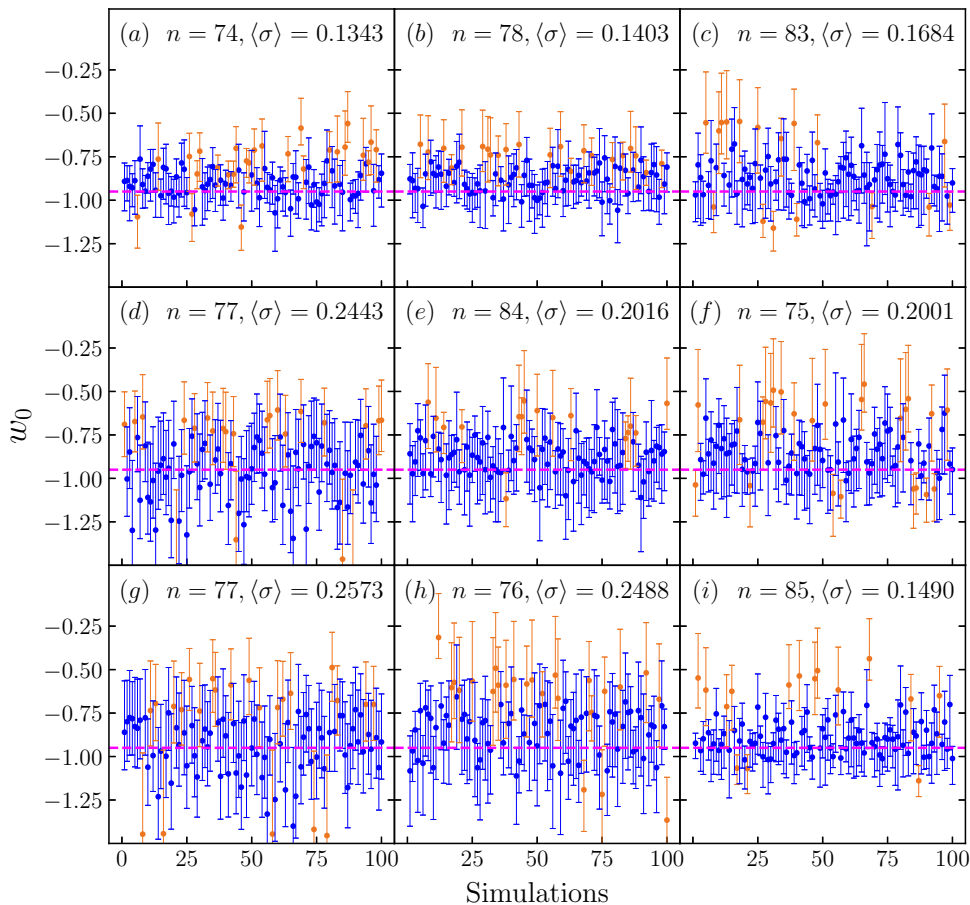


FIG. 9: The same as in Fig. 8, but the marginalized 1σ constraints are on the cosmological parameter w_0 .

cases of the 9 redshift distributions. However, the insight about the constraining ability keeps unchanged. The FRBs simulated with the redshift distributions PzGRB/PzSFR/Uniform, Pzconst(0.5)/PzSFH(0.5), Burr/Burr12/Pzconst(1.0)/PzSFH(1.0) have strong, weak, moderate constraining abilities, respectively. These three groups of redshift distributions lead to different cosmological constraining abilities from the simulated FRBs. Using FRB simulations with different redshift distributions, one will make optimistic, pessimistic, or moderate predictions about the future of the FRB cosmology.

Let us turn to other cosmological models to see whether or not the above insight changes. The second is the flat w CDM model, in which the dimensionless Hubble parameter is given by (e.g. [82, 83])

$$E(z) = \left[\Omega_m(1+z)^3 + (1-\Omega_m)(1+z)^{3(1+w)} \right]^{1/2}, \quad (24)$$

where Ω_m and w are free cosmological parameters. We simulate N_{FRB} FRBs with the preset cosmological parameter $\Omega_m = 0.3153$ and $w = -0.95$. Then, we constrain the flat w CDM model with these simulated FRBs. In Figs. 6 and 7, the marginalized 1σ constraints on the cosmological parameters Ω_m and w are presented, respectively. Since the insight about the constraining ability keeps unchanged when the number of simulated FRBs varies, we only consider the case of $N_{\text{FRB}} = 5000$ for the flat w CDM model. Once again, it is easy to see from Figs. 6 and 7 that both the preset parameters $\Omega_m = 0.3153$ and $w = -0.95$ can be found within 1σ region in most of the 100 simulations, for all cases of the 9 redshift distributions introduced in Sec. II. This implies that the cosmological constraints from simulated FRBs are fairly reliable and robust. On the other hand, since there are two free cosmological parameters Ω_m and w in the flat w CDM model while there is only one cosmological parameter Ω_m in the flat Λ CDM model, the constraints on Ω_m in the flat w CDM model (Fig. 6) are looser than the ones in the Λ CDM model (Fig. 4), as expected. From Figs. 6 and 7, one can find that the cosmological constraints on both Ω_m and w from

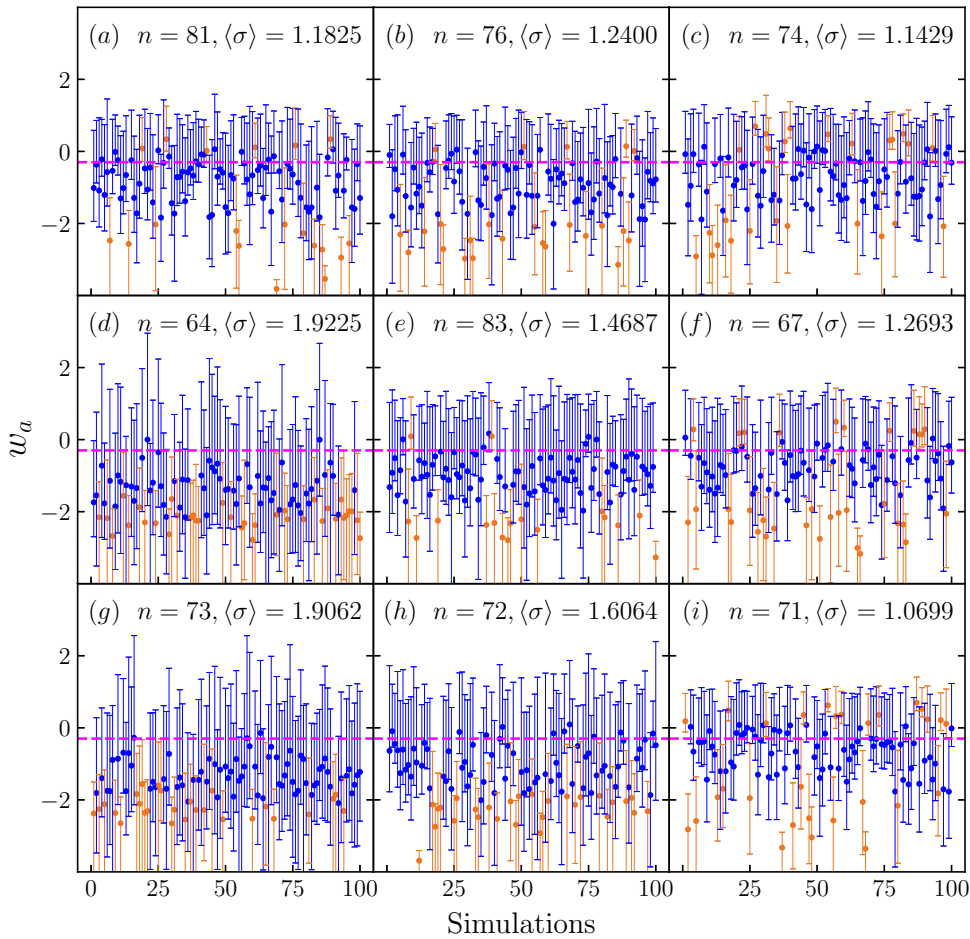


FIG. 10: The same as in Fig. 8, but the marginalized 1σ constraints are on the cosmological parameter w_a .

FRBs simulated with the redshift distributions PzGRB/PzSFR/Uniform, Pzconst(0.5)/PzSFH(0.5), and Burr/Burr12/Pzconst(1.0)/PzSFH(1.0) are tightest, loosest, and moderate, respectively. These three groups of redshift distributions lead to different cosmological constraining abilities from the simulated FRBs. This insight still holds in the case of flat w CDM model.

Finally, we consider the flat Chevallier-Polarski-Linder (CPL) model [84, 85], in which the equation-of-state parameter (EoS) of dark energy is parameterized as

$$w = w_0 + w_a(1 - a) = w_0 + w_a \frac{z}{1+z}, \quad (25)$$

where w_0 and w_a are constants. As is well known, the corresponding $E(z)$ is given by (e.g. [82, 83])

$$E(z) = \left[\Omega_m(1+z)^3 + (1 - \Omega_m)(1+z)^{3(1+w_0+w_a)} \exp\left(-\frac{3w_a z}{1+z}\right) \right]^{1/2}. \quad (26)$$

We simulate N_{FRB} FRBs with the preset parameters $\Omega_m = 0.3153$, $w_0 = -0.95$ and $w_a = -0.3$. Then, we constrain the flat CPL model with these simulated FRBs. Similarly, we only consider the case of $N_{\text{FRB}} = 5000$ for the flat CPL model. In Figs. 8–10, the marginalized 1σ constraints on the cosmological parameters Ω_m , w_0 and w_a are presented, respectively. Again, we find from Figs. 8–10 that the preset cosmological parameters $\Omega_m = 0.3153$, $w_0 = -0.95$ and $w_a = -0.3$ can be found within 1σ region in most of the 100 simulations, for almost all cases of the 9 redshift distributions introduced in Sec. II. There are 3 free cosmological parameters in this model, and hence the cosmological constraints will become worse than the flat Λ CDM and w CDM models which have 1 and 2 free cosmological parameters, respectively. This can be verified by comparing Figs. 8–10 with Figs. 4, 6 and 7.

Let us look at the uncertainties of cosmological constraints. In the case of Ω_m (Fig. 8), the same insight keeps unchanged as in the flat Λ CDM and w CDM models, namely the cosmological constraints on Ω_m from FRBs simulated with the redshift distributions PzGRB/PzSFR/Uniform, Pzconst(0.5)/PzSFH(0.5), and Burr/Burr12/Pzconst(1.0)/PzSFH(1.0) are tightest, loosest, and moderate, respectively.

However, it is slightly changed in the cases of w_0 and w_a . The tightest, loosest, and moderate groups are changed to the distributions Burr/Burr12/PzGRB/Uniform, Pzconst(0.5)/PzSFH(0.5)/PzSFH(1.0), and Pzconst(1.0)/PzSFR in the case of w_0 (Fig. 9), respectively. On the other hand, the tightest, loosest, and moderate groups are changed to the distributions Burr/Burr12/PzGRB/PzSFR/Uniform, Pzconst(0.5)/PzSFH(0.5), and Pzconst(1.0)/PzSFH(1.0) in the case of w_a (Fig. 10), respectively. This is mainly due to the correlation between the cosmological parameters w_0 and w_a .

Nevertheless, it is still unchanged that different redshift distributions lead to different cosmological constraining abilities from the simulated FRBs. Thus, if one uses the unsuitable redshift distributions to simulate FRBs, rather than the actual one of FRBs (which is still unknown to date), overoptimistic or overpessimistic predictions about the future of the FRB cosmology might be made.

V. CONCLUDING REMARKS

Nowadays, FRBs have been a promising probe for astronomy and cosmology. However, it is not easy to identify the redshifts of FRBs to date. Thus, no sufficient actual FRBs with identified redshifts can be used to study cosmology currently. In the past years, one has to use the simulated FRBs with “known” redshifts instead. To simulate an FRB, one should randomly assign a redshift to it from a given redshift distribution. But the actual redshift distribution of FRBs is still unknown so far. Therefore, various redshift distributions have been assumed in the literature, while some of them are motivated by the star formation history/rate or compact binary mergers and so on, some of them are borrowed from other objects such as gamma-ray bursts (GRBs), some of them come from the observed FRBs, and some of them are not well motivated at all. In the present work, we study the effect of various redshift distributions on cosmological constraints, and we do not care whether these redshift distributions are well motivated or where they come from. Our goal is just to see how they affect the cosmological constraints, while they are treated equally in this work, no matter whether they are the intrinsic ones or the observed ones. We find that different redshift distributions lead to different cosmological constraining abilities from the simulated FRBs. This result emphasizes the importance to find the actual redshift distribution of FRBs, and reminds us of the possible bias in the FRB simulations due to the redshift distributions.

In fact, one should also include the contribution from Galactic halos into DM_{obs} in Eq. (2). Although it is poorly known, $DM_{\text{MW, halo}} \approx 50 \sim 80 \text{ pc cm}^{-3}$ was suggested in e.g. [87]. Actually, $DM_{\text{MW, halo}}$ can be absorbed into DM_{MW} and then Eq. (2) takes the same form (but with a different meaning for DM_{MW}), because we only use the extragalactic DM (namely $DM_{\text{E}} \equiv DM_{\text{IGM}} + DM_{\text{HG}}$ as defined in Eq. (3)) to constrain the cosmological models.

We stress that there are other types of redshift distributions for FRBs in the literature. We do not try to consider all redshift distributions for FRBs in a limited work. However, it is expected that our main conclusion will not change for the other redshift distributions unused in this work.

As mentioned above, the 9 redshift distributions can be separated into three distinct groups, namely PzGRB/PzSFR/Uniform, Pzconst(0.5)/PzSFH(0.5), and Burr/Burr12/Pzconst(1.0)/PzSFH(1.0), which lead to strong, weak, and moderate constraining abilities, respectively. In fact, we can find some clues from the left panel of Fig. 2. The normalized redshift distributions PzGRB/PzSFR/Uniform are commonly “short and wide”, and hence the simulated FRBs span almost the whole redshift range from 0 to 3. On the contrary, the normalized redshift distributions Pzconst(0.5)/PzSFH(0.5) are commonly “tall and thin” with a sharp peak nearby the low redshift 0.5, and hence the simulated FRBs concentrate in a narrow redshift range around the redshift 0.5 (in fact it is rare to have redshifts > 1). On the other hand, the normalized redshift distributions Pzconst(1.0)/PzSFH(1.0) are moderate, and hence the simulated FRBs span a fairly wide redshift range from 0 to ~ 2.2 . Although the normalized redshift distributions Burr/Burr12 tilt to low redshifts < 1 , they have not so small probability to generate redshifts in the range from 1 to 2. In this sense, Burr/Burr12 are similar to Pzconst(1.0)/PzSFH(1.0), so that they are also in the moderate group. These are clues found from the left panel of Fig. 2. Naively, we try to understand them as follows. For FRBs at high redshifts, DM_{E} is dominated by the contribution from

IGM, namely DM_{IGM} , which carries the key information about IGM and the cosmic expansion history. In this case, the contribution from host galaxy, $DM_{\text{HG}} = DM_{\text{HG,loc}}/(1+z)$, becomes relatively small. So, it is expected that the constraints on the cosmic expansion history accordingly become tight. Thus, the redshift distributions having larger probability to generate redshifts > 2 or > 1 lead to stronger cosmological constraining abilities (smaller uncertainties) from the simulated FRBs.

In this work, we have proposed two new redshift distributions, namely Burr and Burr12, from the observed FRBs to date. It should be emphasized that the observed redshift distributions is a convolution of the intrinsic redshift distribution (which is unknown so far), the FRB luminosity/energy distribution (which is also unknown), and the sensitivity of telescopes (we thank the referee for pointing out this issue). On the other hand, many selection effects exist in the observed FRBs from different telescopes. Thus, Burr and Burr12 redshift distributions cannot be taken seriously, and cannot be mixed with the intrinsic redshift distribution (which is unknown so far). However, even if we remove Burr, Burr12 and Uniform from the 9 redshift distributions considered in this work, the other 6 redshift distributions still lead to the same conclusion. They are still separated into three distinct groups, namely PzGRB/PzSFR, Pzconst(0.5)/PzSFH(0.5), and Pzconst(1.0)/PzSFH(1.0), without taking Burr, Burr12 and Uniform into account. Although all of the other 6 redshift distributions come from some intrinsic redshift distribution models such as star formation history, they still lead to distinct cosmological constraints, as shown in the present work. Burr and Burr12 are not in the center of this work, and they also cannot change the central conclusion. In fact, some authors used various redshift distributions (such as PzGRB, PzSFR, Pzconst and PzSFH) to simulate FRBs and accordingly considered the constraints on cosmological models in the literature. They made some claims with one of these assumed redshift distributions (such as PzGRB, PzSFR, Pzconst and PzSFH). Our point is that such kind of claims in the literature considerably depend on the assumed redshift distributions. We follow their steps but with various assumed redshift distributions, and find that different redshift distributions lead to different claims. So, such kind of works in the literature are not robust, since there is bias in their claims. This is our key point. To this problem, the key is to find the actual intrinsic redshift distribution of FRBs, which is still unknown to date. We hope that it will be available in the near future. Of course, one can still make some helpful efforts in this direction. For example, in e.g. [88, 89], several intrinsic redshift distribution models (tracking the star formation history/rate or compact binary mergers and so on) were tested with the observational data, and found that they are consistent with these data currently. We consider this is an important topic in the field of FRBs, especially for the FRB cosmology.

ACKNOWLEDGEMENTS

We thank the anonymous referee for quite useful comments and suggestions, which helped us to improve this work. We are grateful to Hua-Kai Deng, Shu-Ling Li, Zhong-Xi Yu, Han-Yue Guo and Jing-Yi Jia for kind help and useful discussions. This work was supported in part by NSFC under Grants No. 11975046 and No. 11575022.

-
- [1] <https://www.nature.com/collections/rswtktxcln>
 - [2] D. R. Lorimer, *Nat. Astron.* **2**, 860 (2018) [arXiv:1811.00195].
 - [3] E. F. Keane, *Nat. Astron.* **2**, 865 (2018) [arXiv:1811.00899].
 - [4] S. R. Kulkarni, *Nat. Astron.* **2**, 832 (2018) [arXiv:1811.00448].
 - [5] J. P. Macquart, *Nat. Astron.* **2**, 836 (2018) [arXiv:1811.00197].
 - [6] S. Burke-Spolaor, *Nat. Astron.* **2**, 845 (2018) [arXiv:1811.00194].
 - [7] U. L. Pen, *Nat. Astron.* **2**, 842 (2018) [arXiv:1811.00605].
 - [8] M. Caleb, L. G. Spitler and B. W. Stappers, *Nat. Astron.* **2**, 839 (2018) [arXiv:1811.00360].
 - [9] B. Zhang, *Nature* **587**, 45 (2020) [arXiv:2011.03500].
 - [10] D. Xiao, F. Wang and Z. Dai, *Sci. China Phys. Mech. Astron.* **64**, 249501 (2021) [arXiv:2101.04907].
 - [11] E. Petroff, J. W. T. Hessels and D. R. Lorimer, *Astron. Astrophys. Rev.* **27**, 4 (2019) [arXiv:1904.07947].
 - [12] J. M. Cordes and S. Chatterjee, *Ann. Rev. Astron. Astrophys.* **57**, 417 (2019) [arXiv:1906.05878].
 - [13] D. R. Lorimer *et al.*, *Science* **318**, 777 (2007) [arXiv:0709.4301].

- [14] D. Thornton *et al.*, *Science* **341**, no. 6141, 53 (2013) [arXiv:1307.1628].
- [15] S. P. Tendulkar *et al.*, *Astrophys. J.* **834**, no. 2, L7 (2017) [arXiv:1701.01100].
- [16] K. W. Bannister *et al.*, *Science* **365**, no. 6453, 565 (2019) [arXiv:1906.11476].
- [17] V. Ravi *et al.*, *Nature* **572**, no. 7769, 352 (2019) [arXiv:1907.01542].
- [18] B. Marcote *et al.*, *Nature* **577**, no. 7789, 190 (2020) [arXiv:2001.02222].
- [19] K. E. Heintz *et al.*, *Astrophys. J.* **903**, no. 2, 152 (2020) [arXiv:2009.10747].
- [20] J.-P. Macquart *et al.*, *Nature* **581**, no. 7809, 391 (2020) [arXiv:2005.13161].
- [21] S. Bhandari *et al.*, *Astrophys. J. Lett.* **901**, no. 2, L20 (2020) [arXiv:2008.12488].
- [22] J. X. Prochaska *et al.*, *Science* **366**, no. 6462, 231 (2019) [arXiv:1909.11681].
- [23] A. J. Batten *et al.*, arXiv:2011.14547 [astro-ph.CO].
- [24] W. Deng and B. Zhang, *Astrophys. J.* **783**, L35 (2014) [arXiv:1401.0059].
- [25] Y. P. Yang and B. Zhang, *Astrophys. J.* **830**, no. 2, L31 (2016) [arXiv:1608.08154].
- [26] H. Gao, Z. Li and B. Zhang, *Astrophys. J.* **788**, 189 (2014) [arXiv:1402.2498].
- [27] B. Zhou, X. Li, T. Wang, Y. Z. Fan and D. M. Wei, *Phys. Rev. D* **89**, 107303 (2014) [arXiv:1401.2927].
- [28] Y. P. Yang, R. Luo, Z. Li and B. Zhang, *Astrophys. J.* **839**, no. 2, L25 (2017) [arXiv:1701.06465].
- [29] H. Yu and F. Y. Wang, *Astron. Astrophys.* **606**, A3 (2017) [arXiv:1708.06905].
- [30] J. J. Wei, X. F. Wu and H. Gao, *Astrophys. J.* **860**, no. 1, L7 (2018) [arXiv:1805.12265].
- [31] Z. X. Li, H. Gao, X. H. Ding, G. J. Wang and B. Zhang, *Nat. Comm.* **9**, 3833 (2018) [arXiv:1708.06357].
- [32] M. Jaroszynski, *Mon. Not. Roy. Astron. Soc.* **484**, no. 2, 1637 (2019) [arXiv:1812.11936].
- [33] M. S. Madhavacheril *et al.*, *Phys. Rev. D* **100**, no. 10, 103532 (2019) [arXiv:1901.02418].
- [34] A. Walters *et al.*, *Astrophys. J.* **856**, no. 1, 65 (2018) [arXiv:1711.11277].
- [35] D. C. Qiang, H. K. Deng and H. Wei, *Class. Quant. Grav.* **37**, no. 18, 185022 (2020) [arXiv:1902.03580].
- [36] D. C. Qiang and H. Wei, *JCAP* **2004**, 023 (2020) [arXiv:2002.10189].
- [37] Z. X. Li *et al.*, *Astrophys. J.* **876**, no. 2, 146 (2019) [arXiv:1904.08927].
- [38] J. J. Wei *et al.*, *JCAP* **1909**, 039 (2019) [arXiv:1907.09772].
- [39] R. G. Cai, T. B. Liu, S. J. Wang and W. T. Xu, *JCAP* **1909**, 016 (2019) [arXiv:1905.01803].
- [40] Y. K. Wang and F. Y. Wang, *Astron. Astrophys.* **614**, A50 (2018) [arXiv:1801.07360].
- [41] G. B. Rybicki and A. P. Lightman, *Radiative Processes in Astrophysics*, John Wiley & Sons, Inc. (1979).
- [42] K. Ioka, *Astrophys. J.* **598**, L79 (2003) [astro-ph/0309200].
- [43] S. Inoue, *Mon. Not. Roy. Astron. Soc.* **348**, 999 (2004) [astro-ph/0309364].
- [44] J. M. Cordes and T. J. W. Lazio, astro-ph/0207156.
- [45] J. M. Cordes and T. J. W. Lazio, astro-ph/0301598.
- [46] J. M. Yao, R. N. Manchester and N. Wang, *Astrophys. J.* **835**, 29 (2017) [arXiv:1610.09448].
- [47] E. Petroff *et al.*, *Publ. Astron. Soc. Austral.* **33**, e045 (2016) [arXiv:1601.03547];
The up-to-date FRB Catalogue is available at <http://www.frbcat.org>
- [48] T. Hashimoto *et al.*, *Mon. Not. Roy. Astron. Soc.* **488**, no. 2, 1908 (2019) [arXiv:1907.11730].
- [49] R. M. Shannon *et al.*, *Nature* **562**, no. 7727, 386 (2018).
- [50] N. Aghanim *et al.*, *Astron. Astrophys.* **641**, A6 (2020) [arXiv:1807.06209].
- [51] B. C. Andersen *et al.*, *Nature* **587**, no. 7832, 54 (2020) [arXiv:2005.10324].
- [52] C. D. Bochenek *et al.*, *Nature* **587**, no. 7832, 59 (2020) [arXiv:2005.10828].
- [53] L. Lin *et al.*, *Nature* **587**, no. 7832, 63 (2020) [arXiv:2005.11479].
- [54] C. K. Li *et al.*, *Nat. Astron.* **5**, 378 (2021) [arXiv:2005.11071].
- [55] <https://pypi.org/project/fitter/>
- [56] <https://scipy.org>
- [57] <https://docs.scipy.org/doc/scipy/reference/generated/scipy.stats.burr.html>
- [58] <https://docs.scipy.org/doc/scipy/reference/generated/scipy.stats.burr12.html>
- [59] L. Shao *et al.*, *Astrophys. J.* **738**, 19 (2011) [arXiv:1104.5498].
- [60] https://en.wikipedia.org/wiki/Erlang_distribution
- [61] J. B. Muñoz *et al.*, *Phys. Rev. Lett.* **117**, no. 9, 091301 (2016) [arXiv:1605.00008].
- [62] M. Caleb *et al.*, *Mon. Not. Roy. Astron. Soc.* **458**, no. 1, 708 (2016) [arXiv:1512.02738].
- [63] S. Cole *et al.*, *Mon. Not. Roy. Astron. Soc.* **326**, 255 (2001) [astro-ph/0012429].
- [64] A. M. Hopkins and J. F. Beacom, *Astrophys. J.* **651**, 142 (2006) [astro-ph/0601463].
- [65] M. Bhattacharya, P. Kumar and E. V. Linder, arXiv:2010.14530 [astro-ph.CO].
- [66] P. Madau and M. Dickinson, *Ann. Rev. Astron. Astrophys.* **52**, 415 (2014) [arXiv:1403.0007].
- [67] M. Fukugita, C. J. Hogan and P. J. E. Peebles, *Astrophys. J.* **503**, 518 (1998) [astro-ph/9712020].
- [68] J. M. Shull, B. D. Smith and C. W. Danforth, *Astrophys. J.* **759**, 23 (2012) [arXiv:1112.2706].
- [69] A. A. Meiksin, *Rev. Mod. Phys.* **81**, 1405 (2009) [arXiv:0711.3358].
- [70] G. D. Becker *et al.*, *Mon. Not. Roy. Astron. Soc.* **410**, 1096 (2011) [arXiv:1008.2622].
- [71] J. M. Shull *et al.*, *Astrophys. J.* **722**, no. 2, 1312 (2010) [arXiv:1008.2957].
- [72] M. McQuinn, *Astrophys. J.* **780**, L33 (2014) [arXiv:1309.4451].

- [73] G. Q. Zhang, H. Yu, J. H. He and F. Y. Wang, *Astrophys. J.* **900**, 170 (2020) [arXiv:2007.13935].
- [74] S. Bhandari *et al.*, *Mon. Not. Roy. Astron. Soc.* **475**, no. 2, 1427 (2018) [arXiv:1711.08110].
- [75] M. Amiri *et al.*, *Nature* **566**, no. 7743, 230 (2019) [arXiv:1901.04524].
- [76] J. Kocz *et al.*, *Mon. Not. Roy. Astron. Soc.* **489**, no. 1, 919 (2019) [arXiv:1906.08699].
- [77] G. Hallinan *et al.*, arXiv:1907.07648 [astro-ph.IM].
- [78] F. Jankowski *et al.*, arXiv:2012.05173 [astro-ph.IM].
- [79] M. Bailes *et al.*, *Publ. Astron. Soc. Austral.* **34**, e045 (2017) [arXiv:1708.09619].
- [80] M. P. van Haarlem *et al.*, *Astron. Astrophys.* **556**, A2 (2013) [arXiv:1305.3550].
- [81] A. Lewis and S. Bridle, *Phys. Rev. D* **66**, 103511 (2002) [astro-ph/0205436], available at <http://cosmologist.info/cosmomc/>
- [82] H. Wei, *JCAP* **1008**, 020 (2010) [arXiv:1004.4951].
- [83] J. Liu and H. Wei, *Gen. Rel. Grav.* **47**, no. 11, 141 (2015) [arXiv:1410.3960].
- [84] M. Chevallier and D. Polarski, *Int. J. Mod. Phys. D* **10**, 213 (2001) [gr-qc/0009008].
- [85] E. V. Linder, *Phys. Rev. Lett.* **90**, 091301 (2003) [astro-ph/0208512].
- [86] P. Beniamini *et al.*, *Mon. Not. Roy. Astron. Soc.* **502**, no. 4, 5134 (2021) [arXiv:2011.11643].
- [87] J. X. Prochaska and Y. Zheng, *Mon. Not. Roy. Astron. Soc.* **485**, no. 1, 648 (2019) [arXiv:1901.11051].
- [88] R. C. Zhang *et al.*, *Mon. Not. Roy. Astron. Soc.* **501**, no. 1, 157 (2021) [arXiv:2011.06151].
- [89] C. W. James *et al.*, arXiv:2101.07998 [astro-ph.HE].